Journal of the Egyptian Mathematical Society (2012) **20**, 139–151

Egyptian Mathematical Society

Journal of the Egyptian Mathematical Society

www.etms-eg.org
www.elsevier.com/locate/joems

ORIGINAL ARTICLE

Numerical study of viscous dissipation effect on free convection heat and mass transfer of MHD non-Newtonian fluid flow through a porous medium

Nabil T.M. Eldabe *, Sallam N. Sallam, Mohamed Y. Abou-zeid

Department of Mathematics, Faculty of Education, Ain Shams University, Heliopolis, Cairo, Egypt

Received 15 August 2011; revised 10 June 2012
Available online 22 October 2012

KEYWORDS

Non-Newtonian;
Heat and mass transfer;
Viscous dissipation;
Porous medium

Abstract The problem of free convection heat with mass transfer for MHD non-Newtonian Eyring–Powell flow through a porous medium, over an infinite vertical plate is studied. Taking into account the effects of both viscous dissipation and heat source. The temperature and concentration are of periodic variation. The governing non-linear partial differential equations of this phenomenon are transformed into non-linear algebraic system utilizing finite difference method. Numerical results for the velocity, temperature and concentration distributions as well as the skin friction, heat and mass transfer are obtained and reported in tabular form and graphically for different values of physical parameters of the problem. Also, the stability condition is studied.

1. Introduction

The most common type of body force, which acts on a fluid, is due to gravity, so that the body force can be defined as in magnitude and direction by the acceleration due to gravity. Sometimes, electromagnetic effects are important. The electric and magnetic fields themselves must obey a set of physical laws, which are expressed by Maxwells equations. The solution of such problems requires the simultaneous solution of the equations of fluid mechanics and electromagnetism. One special case of this type of coupling is known as magnetohydrodynamic.

Coupled heat and mass transfer phenomenon in porous media is gaining attention due to its interesting applications. The flow phenomenon in this case is relatively complex than that in pure thermal/solutal convection process. Processes involving heat and mass transfer in porous media are often encountered in the chemical industry, in reservoir engineering in connection with thermal recovery process, in the study of dynamics of hot and salty springs of a sea. Underground spreading of chemical waste and other pollutants, grain storage, evaporation cooling, and solidification are a few other application areas where combined thermosolutal convection in porous media are observed. However, the exhaustive volume of work devoted to this area is amply documented by the most recent books by Ingham and Pop [6], Nield and Bejan

* Corresponding author.
E-mail address: master_math2003@yahoo.com (N.T.M. Eldabe).
Peer review under responsibility of Egyptian Mathematical Society.

ELSEVIER Production and hosting by Elsevier

1110-256X © 2012 Egyptian Mathematical Society. Production and hosting by Elsevier B.V. Open access under CC BY-NC-ND license.
http://dx.doi.org/10.1016/j.joems.2012.08.013

Nomenclature

a and b	characteristics of Eyring–Powell model
B_0	strength of uniform magnetic field
C	concentration of the species
C_E	Ergun constant
C_p	specific heat at constant pressure
C_s	concentration susceptibilty
D_a	Darcy number $= \frac{K}{\nu t_R}$
D_f	Dufour number $= \frac{D\Delta CK_T}{\nu C_s C_p (T_\omega - T_\infty)}$
D	coefficient of mass diffusivity
E_c	Eckert number $= \frac{U_0^2}{C_p(T_\omega - T_\infty)}$
g_o	gravity acceleration
I	$\sqrt{-1}$
k	thermal conductivity
K	permeability constant
K_T	thermal diffusion ratio
M	magnetic parameter $= \frac{\sigma B_0^2 t_R}{\rho}$
N	(buoyancy ratio)$= \frac{\beta^\star \Delta C}{\beta(T_\omega - T_\infty)}$
P_r	Prandtl number $\frac{\nu \rho C_p}{k}$
Q_0	volumetric rate of heat generation
S_c	Schmidt number $= \frac{\nu}{D}$
S_r	Soret number $= \frac{DK_t \Delta T}{\nu T_m \Delta C}$
t	time
T	temperature of the fluid
T_m	the mean temperature
V_i	velocity vector $= (u(y,t),0,0)$

Greek symbols

$\hat{\alpha}$	non-dimensional parameter $= \frac{t_R}{\rho a b L_R^2}$
β	volumetric coefficient of thermal expansion
$\beta^\star$	volumetric of expansion with concentration
δ	non-dimensional parameter $= \frac{\sqrt{\gamma}}{\hat{\alpha}}$
γ	non-dimensional parameter $= \frac{u_R^2}{a^2 L_r^2}$
μ	viscosity
ν	kinematic viscosity $= \frac{\mu}{\rho}$
ω	frequency of the oscillating plate
ρ	density of the species
σ	electrical conductivity of the fluid
Γ	stress tensor in the Eyring–Powell model

Superscripts and subscripts

∞	free stream condition
ω	wall or plate condition

[9] and Vafai [15], Pop and Ingham [10] studied the problem of transient flow of a fluid past a moving semi-infinite vertical porous plate. However, many problem areas which are important in applications, as well as in theory still persist.

Trevisan and Bejan [14] have studied the problem of combined heat and mass transfer by free convection in a porous medium. They studied the natural convection phenomenon occurring inside a porous layer with both heat and mass transfer from the side and derived the natural circulation by a combination of buoyancy effects due to both temperature and concentration variations. The problem of convective heat transfer in an electrically conducting fluid at a stretching surface with uniform free stream is investigated by Vajravelu and Hadjinicolaou [16]. Abd El-naby et al. [1] carried out the finite difference method for the problem of radiation effects on MHD unsteady free-convection flow over vertical plate with variable surface temperature. The problem of flow of a micropolar fluid past a moving semi-infinite vertical porous plate with mixed radiative convection is studied by Kim and Fedorov [8]. Kafoussias [7] discussed the effects of mass transfer on free convective flow of a viscous fluid past a vertical isothermal cone surface. He obtained the effects of the buoyancy parameter and Schmidt number on the flow field. Seddeek [11] discussed the problem of thermal radiation and buoyancy effects on MHD free convective heat generating flow over an accelerating permeable surface with temperature-dependent viscosity.

Eldabe [4] studied the problem of free convective flow through a porous medium bounded by an infinite, porous, vertical plate whose temperature fluctuates harmonically with time from a constant mean. The method of implicit finite difference analysis of transient free convective flow past a semi infinite vertical flat plate with mass transfer was carried out by Soundalgekar and Ganesan [13]. Eldabe et al. [3,5] presented numerical solutions for the problem of unsteady flow of a magnetohydrodynamic convective heat and mass transfer in an electrically conducting fluid over an infinite solid surface and unsteady flow of an electrically conducting non-Newtonian fluid (Eyring–Powell model) past a porous plate through a non-Darcy porous medium with heat and mass transfer in the presence of viscous and Joulean dissipations. The plate is oscillating in its own plane with superimposed injection or suction. They took into consideration a uniform magnetic field and internal heat generation.

The aim of this work is to study the thermaldiffusion and diffusionthermo effects on free convective heat with mass transfer of flow of an electrically conducting Eyring–Powell incompressible fluid through a porous media. This fluid is flowing past an infinite vertical plate under periodic plate temperature/concentration with frequency ω. Also, we take into our consideration the effects of transverse magnetic field with a uniform intensity as well as the effects of both viscous dissipation and internal heat generation. After transforming the system of non-linear partial differential equations which governs the problem into algebraic system of non-linear equations by using finite difference method, the numerical formulas for the velocity, temperature and concentration as well as the skin friction, the rate of heat and mass transfer are obtained.

Therefore, the main idea of the present work is to make a mathematical modeling of this phenomenon and the out purpose is to find the relation between the different parameters and the external forces with the solutions of the problem.

2. Mathematical formulation

We choose the Eyring–Powell model, Eldabe [5], to describe the non-Newtonian fluid, which is in the usual notation given as:

$$\Gamma_v = \mu \frac{\partial v_i}{\partial x_j} + \frac{1}{b} sinh^{-1}\left(\frac{1}{a}\frac{\partial V_i}{\partial x_j}\right) \tag{1}$$

Consider the infinite vertical plate embeded an infinite mass of the fluid. Initially the temperature and concentration of both being assumed at T_∞ and C_∞. At time $t > 0$, the plate temperature and concentration are raised to T_ω and C_ω, and a periodic temperature and/concentration are assumed to be superimposed on this mean constant temperature/concentration of the plate (see Figure 1). A magnetic field of uniform strength B_0 is applied transversally to the direction of the flow. The magnetic Reynold's number of the flow is taken to be small enough so that the induced magnetic field can be neglected. The origin of the coordinate system is taken to be at any point of the flat vertical infinite plate, the x-axis is chosen along the plate vertically upwards, and the y-axis perpendicular to the plate. The problem is governed by the following set of equations, Eldabe et al. [3] and Eckert and Drake [2].

$$\frac{\partial u}{\partial t} = \nu \frac{\partial^2 u}{\partial y^2} + \frac{1}{\rho ab}\left(\frac{\partial^2 u}{\partial y^2}\right) \frac{1}{\sqrt{\frac{1}{a^2}\left(\frac{\partial u}{\partial y}\right)^2 + 1}} - \left(\frac{\sigma B_0^2}{\rho} + \frac{\nu}{K}\right) u + g_0\beta(T - T_\infty) + g_0 B^\star (C - C_\infty) \tag{2}$$

$$\frac{\partial T}{\partial t} = \frac{k}{\rho C_p}\frac{\partial^2 T}{\partial y^2} + \frac{\nu}{C_p}\left(\frac{\partial u}{\partial y}\right)^2 + \frac{1}{\rho b C_p}\left(\frac{\partial u}{\partial y}\right) sinh^{-1}\left(\frac{1}{a}\frac{\partial u}{\partial y}\right) + \frac{\sigma B_0^2 u^2}{\rho C_p} + \frac{D_m K_T}{C_p C_s}\frac{\partial^2 C}{\partial y^2} + Q_0(T - T_\infty) \tag{3}$$

$$\frac{\partial C}{\partial t} = D\frac{\partial^2 C}{\partial y^2} + \frac{D_m K_T}{T_m}\frac{\partial^2 T}{\partial y^2} \tag{4}$$

with the following initial and boundary conditions

$$\begin{cases} u = 0, \quad T = T_\infty, \quad C = C_\infty \quad for\ all \quad t \leqslant 0 \\ u = 0, \quad T = T_\infty + \epsilon(T_\omega - T_\infty) cos\omega t \\ C = C_\infty + \epsilon(C_\omega - C_\infty) cos\omega t, \quad at \quad y = 0, \quad t > 0 \\ \text{and } u \to 0, \quad T \to T_\infty, \quad C \to C_\infty \quad as \quad y \to \infty, \quad t > 0 \end{cases} \tag{5}$$

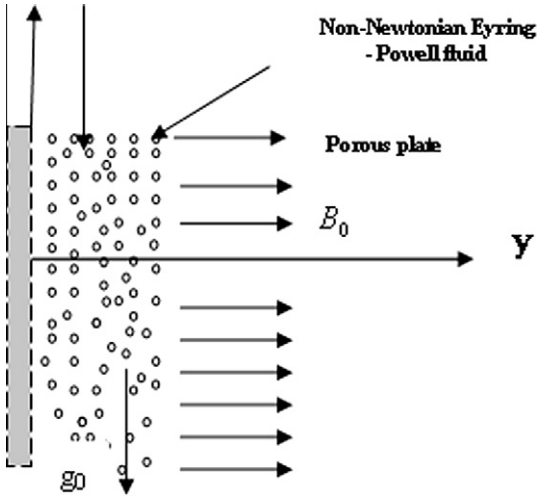

Figure 1 Sketch of the diagram.

Let us introduce the following dimensionless quantities:

$$t^\star = \frac{t}{t_R}, \quad \omega^\star = t_R\omega, \quad \eta = \frac{y}{L_R}, \quad f = \frac{u}{u_R}$$
$$\theta = \frac{T - T_\infty}{T_\omega - T_\infty}, \quad \phi = \frac{C - C_\infty}{C_\omega - C_\infty}, \quad Q_0^\star = Q_0 t_R \tag{6}$$

where

$$u_R = (\nu g_0 \beta \Delta T)^{\frac{1}{3}}, \quad L_R = \left(\frac{g_0\beta\Delta T}{\nu^2}\right)^{\frac{1}{3}} \text{ and } t_R = (g_0\beta\Delta T)^{-\frac{2}{3}}\nu^{\frac{1}{3}} \tag{7}$$

The Eqs. (2)–(4) and the boundary conditions (5) are obtained in the dimensionless form after dropping the star mark as follows:

$$\frac{\partial f}{\partial t} = \left(1 + \frac{\hat{\alpha}}{\sqrt{\gamma\left(\frac{\partial f}{\partial \eta}\right)^2 + 1}}\right)\frac{\partial^2 f}{\partial \eta^2} - \left(M + \frac{1}{Da}\right) f + \theta + N\psi \tag{8}$$

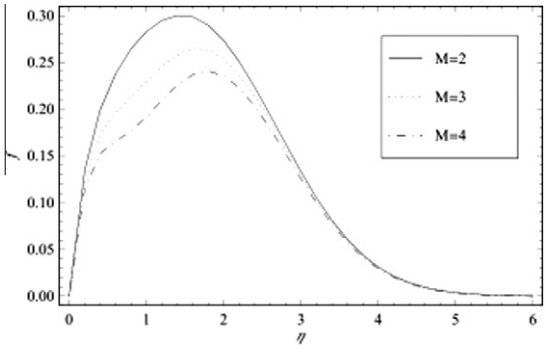

Figure 2 The velocity distribution is plotted vs. η, for a system having the parameters $\epsilon = .1$, $\tau = \frac{\pi}{5}$, $c = 1$, $\alpha = .8$, $\gamma = .4$, $\delta = \sqrt{\frac{\gamma}{\alpha}}$, $M = 2$, $D_a = .15$, $N = 100$, $P_r = 3$, $E_c = 4$, $Q_0 = 1$, $S_c = .5$, $S_r = .3$ and $D_f = .1$ for various values of M.

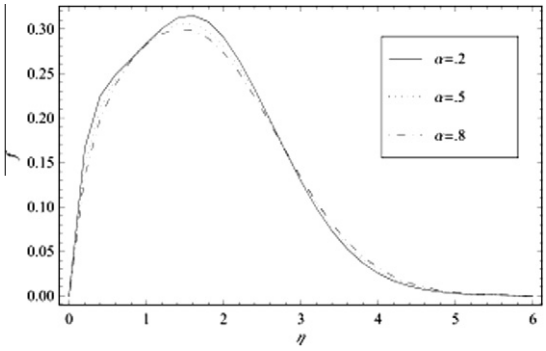

Figure 3 The velocity distribution is plotted vs. η, for a system having the parameters $\epsilon = .1$, $\tau = \frac{\pi}{5}$, $c = 1$, $\alpha = .8$, $\gamma = .4$, $\delta = \sqrt{\frac{\gamma}{\alpha}}$, $M = 2$, $D_a = .15$, $N = 100$, $P_r = 3$, $E_c = 4$, $Q_0 = 1$, $S_c = .5$, $S_r = .3$ and $D_f = .1$ for various values of α.

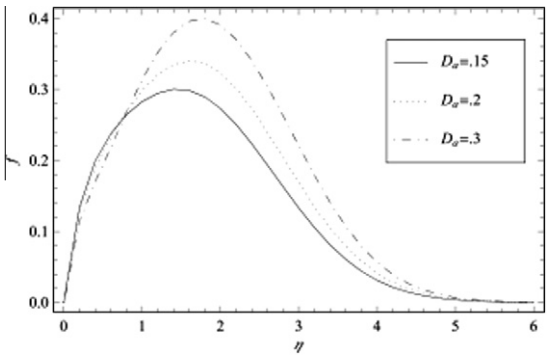

Figure 4 The velocity distribution is plotted vs. η, for a system having the parameters $\epsilon = .1,\ \tau = \frac{\pi}{5},\ c = 1,\ \alpha = .8,\ \gamma = .4,\ \delta = \sqrt{\frac{\gamma}{\alpha}},\ M = 2,\ D_a = .15,\ N = 100,\ P_r = 3,\ E_c = 4,\ Q_0 = 1,\ S_c = .5,\ S_r = .3$ and $D_f = .1$ for various values of D_a.

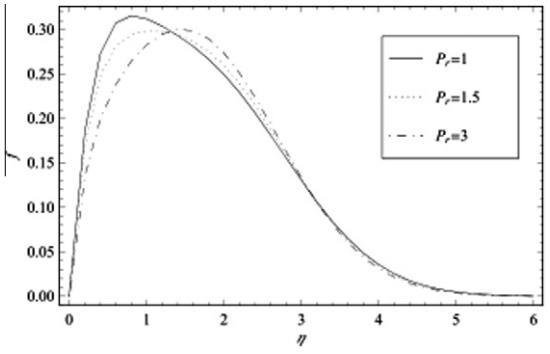

Figure 5 The velocity distribution is plotted vs. η, for a system having the parameters $\epsilon = .1,\ \tau = \frac{\pi}{5},\ c = 1,\ \alpha = .8,\ \gamma = .4,\ \delta = \sqrt{\frac{\gamma}{\alpha}},\ M = 2,\ D_a = .15,\ N = 100,\ P_r = 3,\ E_c = 4,\ Q_0 = 1,\ S_c = .5,\ S_r = .3$ and $D_f = .1$ for various values of P_r.

$$\frac{\partial\theta}{\partial t} = \frac{1}{P_r}\frac{\partial^2\theta}{\partial\eta^2} + E_c\left(\frac{\partial f}{\partial\eta}\right)^2 + \frac{E_c}{\delta}\left(\frac{\partial f}{\partial\eta}\right)sinh^{-1}\left(\sqrt{\gamma}\frac{\partial f}{\partial\eta}\right) + Q_0\theta + D_f\frac{\partial^2\psi}{\partial\eta^2} \tag{9}$$

$$\frac{\partial\psi}{\partial t} = \frac{1}{Sc}\frac{\partial^2\psi}{\partial\eta^2} + Sr\frac{\partial^2\theta}{\partial\eta^2} \tag{10}$$

with initial and boundary conditions

$$\begin{aligned} &f = 0, \quad \theta = 0, \quad \psi = 0 \quad \text{for all} \quad \eta, t \leqslant 0 \\ &f = 0, \quad \theta = \epsilon cos\omega t, \quad \psi = \epsilon cos\omega t, \quad at \quad \eta = 0, \quad t > 0 \\ &and \quad f \to 0, \quad \theta \to 0, \quad \psi \to 0 \quad \text{as} \quad \eta \to \infty, \quad t > 0 \end{aligned} \tag{11}$$

We shall solve the system of non-linear partial differential equations numerically using the finite difference technique and Eqs. (8)–(10) yield.

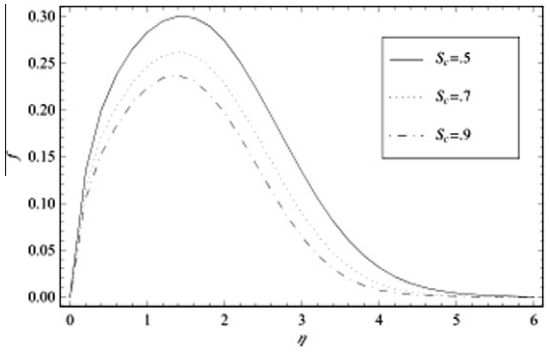

Figure 6 The velocity distribution is plotted vs. η, for a system having the parameters $\epsilon = .1,\ \tau = \frac{\pi}{5},\ c = 1,\ \alpha = .8,\ \gamma = .4,\ \delta = \sqrt{\frac{\gamma}{\alpha}},\ M = 2,\ D_a = .15,\ N = 100,\ P_r = 3,\ E_c = 4,\ Q_0 = 1,\ S_c = .5,\ S_r = .3$ and $D_f = .1$ for various values of S_c.

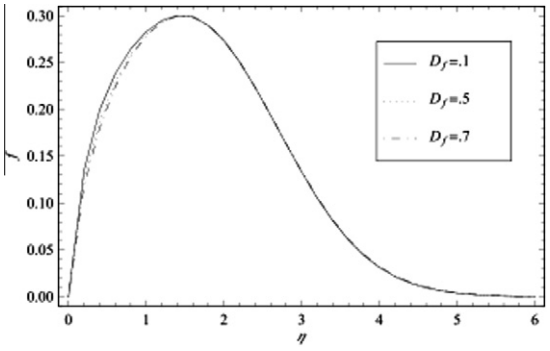

Figure 7 The velocity distribution is plotted vs. η, for a system having the parameters $\epsilon = .1,\ \tau = \frac{\pi}{5},\ c = 1,\ \alpha = .8,\ \gamma = .4,\ \delta = \sqrt{\frac{\gamma}{\alpha}},\ M = 2,\ D_a = .15,\ N = 100,\ P_r = 3,\ E_c = 4,\ Q_0 = 1,\ S_c = .5,\ S_r = .3$ and $D_f = .1$ for various values of D_f.

$$\frac{f_i^{n+1} - f_i^n}{\Delta\tau} = \left(\frac{f_{i+1}^n - 2f_i^n + f_{i-1}^n}{(\Delta\eta)^2}\right)\left(1 + \frac{\hat{\alpha}}{\sqrt{\gamma\left(\frac{f_{i+1}^n - f_i^n}{\Delta\eta}\right)^2 + 1}}\right) - \left(M + \frac{1}{D_a}\right)f_i^n + \theta_i^n + N\psi_i^n \tag{12}$$

$$\frac{\theta_i^{n+1} - \theta_i^n}{\Delta\tau} = \frac{1}{P_r}\left(\frac{\theta_{i+1}^n - 2\theta_i^n + \theta_{i-1}^n}{(\Delta\eta)^2}\right) + E_c\left(\frac{f_{i+1}^n - f_i^n}{\Delta\eta}\right)^2 + ME_c\left(f_i^n\right)^2 + \frac{E_c}{\delta}\left(\frac{f_{i+1}^n - f_i^n}{\Delta\eta}\right)sinh^{-1}\left(\sqrt{\gamma}\left(\frac{f_{i+1}^n - f_i^n}{\Delta\eta}\right)\right) + D_f\left(\frac{\psi_{i+1}^n - 2\psi_i^n + \psi_{i-1}^n}{(\Delta\eta)^2}\right) + Q_0\theta_i^n \tag{13}$$

$$\frac{\psi_i^{n+1} - \psi_i^n}{\Delta\tau} = \frac{1}{S_c}\left(\frac{\psi_{i+1}^n - 2\psi_i^n + \psi_{i-1}^n}{(\Delta\eta)^2}\right) + S_r\left(\frac{\theta_{i+1}^n - 2\theta_i^n + \theta_{i-1}^n}{(\Delta\eta)^2}\right) \tag{14}$$

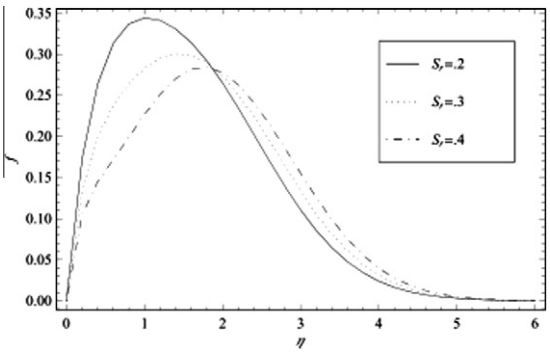

Figure 8 The velocity distribution is plotted vs. η, for a system having the parameters $\epsilon = .1,\ \tau = \frac{\pi}{5},\ c = 1,\ \alpha = .8,\ \gamma = .4,\ \delta = \sqrt{\frac{\gamma}{\alpha}},\ M = 2,\ D_a = .15,\ N = 100,\ P_r = 3,\ E_c = 4,\ Q_0 = 1,\ S_c = .5,\ S_r = .3$ and $D_f = .1$ for various values of S_r.

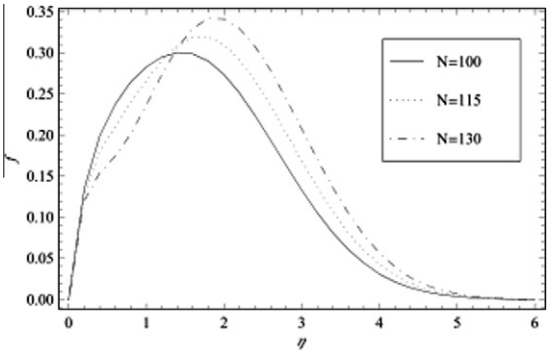

Figure 9 The velocity distribution is plotted vs. η, for a system having the parameters $\epsilon = .1,\ \tau = \frac{\pi}{5},\ c = 1,\ \alpha = .8,\ \gamma = .4,\ \delta = \sqrt{\frac{\gamma}{\alpha}},\ M = 2,\ D_a = .15,\ N = 100,\ P_r = 3,\ E_c = 4,\ Q_0 = 1,\ S_c = .5,\ S_r = .3$ and $D_f = .1$ for various values of N.

where the indices i and n refer to η and t respectively. The initial and boundary conditions (11) yield.

$$\begin{cases} f_i^n = 0,\ \ \theta_i^n = 0,\ \ \psi_i^n = 0 \ \text{ for all } \eta, t \leqslant 0 \\ f_i^n = 0,\ \ \theta_i^n = \epsilon cos\omega(n(\Delta\tau)),\ \ \psi_i^n = \epsilon cos\omega(n(\Delta\tau)),\ \ at\ \ \eta = 0,\ \ t > 0 \\ f_i^n \to 0,\ \ \theta_i^n \to 0,\ \ \psi_i^n \to 0 \ \text{ as } \ \eta \to \infty,\ \ t > 0 \end{cases} \tag{15}$$

3. Consistency of the finite difference scheme

The term consistency applied to a finite difference procedure means that the procedure may in fact approximate the solution of the partial differential equation under study and not the solution of any other partial differential equation. The consistency is measured in terms of the difference between a differential equation and a difference equation. Here, we can write

$$\frac{\partial f}{\partial t} = \frac{f_i^{n+1} - f_i^n}{\Delta\tau} + O(\Delta\tau)$$

$$\frac{\partial \theta}{\partial t} = \frac{\theta_i^{n+1} - \theta_i^n}{\Delta\tau} + O(\Delta\tau)$$

$$\frac{\partial \psi}{\partial t} = \frac{\psi_i^{n+1} - \psi_i^n}{\Delta\tau} + O(\Delta\tau)$$

$$\frac{\partial f}{\partial \eta} = \frac{f_{i+1}^n - f_i^n}{\Delta\eta} + O(\Delta\eta)$$

$$\frac{\partial^2 f}{\partial \eta^2} = \frac{f_{i+1}^n - 2f_i^n + f_{i-1}^n}{(\Delta\eta)^2} + O(\Delta\eta)^2$$

$$\frac{\partial^2 \theta}{\partial \eta^2} = \frac{\theta_{i+1}^n - 2\theta_i^n + \theta_{i-1}^n}{(\Delta\eta)^2} + O(\Delta\eta)^2$$

$$\frac{\partial^2 \psi}{\partial \eta^2} = \frac{\psi_{i+1}^n - 2\psi_i^n + \psi_{i-1}^n}{(\Delta\eta)^2} + O(\Delta\eta)^2$$

For consistency of Eq. (12), we estimate

$$\begin{aligned} &\left\{ \frac{f_i^{n+1} - f_i^n}{\Delta\tau} - \left(\frac{f_{i+1}^n - 2f_i^n + f_{i-1}^n}{(\Delta\eta)^2} \right) \left(1 + \frac{\hat{\alpha}}{\sqrt{\gamma \left(\frac{f_{i+1}^n - f_i^n}{\Delta\eta} \right)^2 + 1}} \right) \right. \\ &\left. + \left(M + \frac{1}{D_a} \right) f_i^n - \theta_i^n - N\psi_i^n \right\} \\ &- \left\{ \frac{\partial f}{\partial t} - \left(1 + \frac{\hat{\alpha}}{\sqrt{\gamma \left(\frac{\partial f}{\partial \eta} \right)^2 + 1}} \right) \frac{\partial^2 f}{\partial \eta^2} + \left(M + \frac{1}{D_a} \right) f - \theta - N\psi_i^n \right\}_{i,n} \\ &= O(\Delta\tau) + O(\Delta\eta) \end{aligned} \tag{16}$$

and for consistency of Eq. (13), we estimate

$$\begin{aligned} &\left\{ \frac{\theta_i^{n+1} - \theta_i^n}{\Delta\tau} - \frac{1}{P_r} \left(\frac{\theta_{n+1}^n - 2\theta_i^n + \theta_{i-1}^n}{(\Delta\eta)^2} \right) - E_c \left(\frac{f_{i+1}^n - f_i^n}{\Delta\eta} \right)^2 - ME_c (f_i^n)^2 \right. \\ &- \frac{E_c}{\delta} \left(\frac{f_{i+1}^n - f_i^n}{\Delta\eta} \right) sinh^{-1} \left(\sqrt{\gamma} \left(\frac{f_{i+1}^n - f_i^n}{\Delta\eta} \right) \right) \\ &\left. - D_f \left(\frac{\psi_{i+1}^n - 2\psi_i^n + \psi_{i-1}^n}{(\Delta\eta)^2} \right) - Q_0 \theta_i^n \right\} \\ &- \left\{ \frac{\partial \theta}{\partial t} - \frac{1}{P_r} \frac{\partial^2 \theta}{\partial \eta^2} \right\} - E_c \left(\frac{\partial f}{\partial \eta} \right)^2 - \frac{E_c}{\delta} \left(\frac{\partial f}{\partial \eta} \right) sinh^{-1} \left(\sqrt{\gamma} \frac{\partial f}{\partial \eta} \right) \\ &\left. - Q_0 \theta - D_f \frac{\partial^2 \psi}{\partial \eta^2} \right\}_{i,n} = O(\Delta\tau) + O(\Delta\eta) \end{aligned} \tag{17}$$

similarly with respect to Eq. (14)

$$\begin{aligned} &\left\{ \frac{\psi_n^{n+1} - \psi_i^n}{\Delta\tau} - \frac{1}{S_c} \left(\frac{\psi_{i+1}^n - 2\psi_i^n + \psi_{i-1}^n}{(\Delta\eta)^2} \right) - S_r \left(\frac{\theta_{i+1}^n - 2\theta_i^n + \theta_{i-1}^n}{(\Delta\eta)^2} \right) \right\} \\ &- \left\{ \frac{\partial \psi}{\partial t} - \frac{1}{Sc} \frac{\partial^2 \psi}{\partial \eta^2} - Sr \frac{\partial^2 \theta}{\partial \eta^2} \right\} = O(\Delta\tau) + O(\Delta\eta) \end{aligned} \tag{18}$$

Here, R.H.S. of Eqs. (16)–(18) represent truncation error as $\Delta\tau \to 0$ with $\Delta\eta \to 0$, the truncation error tends to zero. Hence our explicit scheme is consistent.

4. Stability condition of the scheme

The Von Neumann method is used to study the stability condition for the finite difference equations. Assume a Fourier component for f_i^n, θ_i^n and ψ_i^n as

$$f_i^n = F(\tau)^{Ip(\Delta\eta)i}, \quad \theta_i^n = \Theta(\tau)^{Ip(\Delta\eta)i} \quad \text{and} \quad \psi_i^n = \Psi(\tau)^{Ip(\Delta\eta)i}$$

where p is the wave number in y-direction. Let $\phi = p(\Delta\eta)$ then

$$f_i^n = F(\tau)e^{I\phi i}, \quad \theta_i^n = \Theta(\tau)e^{I\phi i} \quad \text{and} \quad \psi_i^n = \Psi(\tau)e^{I\phi i} \tag{19}$$

Similarly,

$$f_{i\mp1}^n = F(\tau)e^{I\phi(i\mp1)}, \quad \theta_{i\mp1}^n = \Theta(\tau)e^{I\phi(i\mp1)} \quad \text{and} \quad \psi_{i\mp1}^n = \Psi(\tau)e^{I\phi(i\mp1)} \tag{20}$$

and

$$f_i^{n+1} = F(\tau)e^{I\phi i}, \quad \theta_i^{n+1} = \Theta(\tau)e^{I\phi i} \quad \text{and} \quad \psi_i^{n+1} = \Psi(\tau)e^{I\phi i} \tag{21}$$

Substituting Eqs. (19)–(21) into Eqs. (12)–(14) we get

$$\frac{F'-F}{\Delta\tau} = \frac{F(e^{I\phi}-2+e^{-I\phi})}{(\Delta\eta)^2}\left(1+\frac{\hat{\alpha}}{\sqrt{\left|\gamma\frac{f_{i+1}^n-f_i^n}{\Delta\eta}\right|^2+1}}\right) - \left(M+\frac{1}{D_a}\right)F+\Theta+N\Psi \tag{22}$$

$$\frac{\Theta'-\Theta}{\Delta\tau} = \frac{1}{P_r}\left(\frac{\Theta(e^{I\phi}-2+e^{-I\phi})}{(\Delta\eta)^2}\right) + E_c\left|\frac{f_{i+1}^n-f_i^n}{\Delta\eta}\right|\left(\frac{F(e^{I\phi}-1)}{\Delta\eta}\right) + ME_cF|F_i^n| + \frac{E_c}{\delta}\left(\frac{F(e^{I\phi}-1)}{\Delta\eta}\right)sinh^{-1}\left(\sqrt{\gamma}|\frac{f_{i+1}^n-f_i^n}{\Delta\eta}|\right) + D_f\left(\frac{\Psi(e^{I\phi}-2+e^{I\phi})}{(\Delta\eta)^2}\right)+Q_0\Theta \tag{23}$$

$$\frac{\Psi'-\Psi}{\Delta\tau} = \frac{1}{S_c}\left(\frac{\Psi(e^{I\phi}-2+2^{-I\phi})}{(\Delta\eta)^2}\right) + S_r\left(\frac{\Theta(e^{I\phi}-2+e^{-I\phi})}{(\Delta\eta)^2}\right) \tag{24}$$

The Eqs. (22)–(24) can be written as

$$F' = F\left[1+\frac{2(\Delta\tau)}{(\Delta\eta)^2}(cos\phi-1)\left(1+\frac{\hat{\alpha}}{\sqrt{\gamma\left|\frac{f_{i+1}^n-f_i^n}{\Delta\eta}\right|+1}}\right) -(\Delta\tau)\left(M+\frac{1}{D_a}\right)\right]+\Theta+N\Psi \tag{25}$$

$$\Theta' = F\left[E_c\left(\frac{\Delta\tau}{\Delta\eta}\right)(e^{I\phi}-1)\left(\left|\frac{f_{i+1}^n-f_i^n}{\Delta\eta}\right|+\frac{1}{\delta}sinh^{-1}\left(\sqrt{\gamma}\left|\frac{f_{i+1}^n-f_i^n}{\Delta\eta}\right|\right)\right) +(\Delta\tau)ME_c|f_i^n|\right]+\Theta\left[1+\frac{2(\Delta\tau)}{P_r(\Delta\eta)^2}(cos\phi-1)+Q_0\right] +\Psi\left[\frac{2D_f(\Delta\tau)}{(\Delta\eta)^2}(cos\phi-1)\right] \tag{26}$$

$$\Psi' = \Theta\left[\frac{2S_r(\Delta\tau)}{(\Delta\eta)^2}(cos\phi-1)\right]+\Psi\left[1+\frac{2(\Delta\tau)}{S_c(\Delta\eta)^2}(cos\phi-1)\right] \tag{27}$$

The Eqs. (25)–(27) can be written in the form

$$F' = A_1F+A_2\Theta+A_3\Psi \tag{28}$$

$$\Theta' = A_4F+A_5\Theta+A_6\Psi \tag{29}$$

$$\Psi' = A_7\Theta+A_8\Psi \tag{30}$$

where $A_1, A_2, \ldots, A_8$ are defined in the appendix.

The Eqs. (28)–(30) in matrix form can be expressed as follows

$$\begin{pmatrix}F'\\ \Theta'\\ \Psi'\end{pmatrix} = \begin{pmatrix}A_1 & A_2 & A_3\\ A_4 & A_5 & A_6\\ 0 & A_7 & A_8\end{pmatrix}\begin{pmatrix}F\\ \Theta\\ \Psi\end{pmatrix}$$

where the amplification factor is $A = \begin{pmatrix}A_1 & A_2 & A_3\\ A_4 & A_5 & A_6\\ 0 & A_7 & A_8\end{pmatrix}$.

For stability, the modulus of each of the eigenvalue λ_m of the amplification A must not exceed unity. Hence the stability condition is:

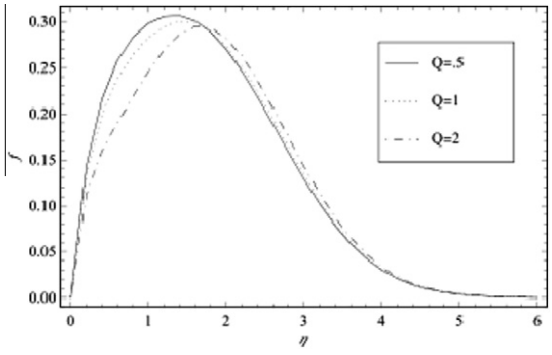

Figure 10 The velocity distribution is plotted vs. η, for a system having the parameters $\epsilon = .1$, $\tau = \frac{\pi}{5}$, $c = 1$, $\alpha = .8$, $\gamma = .4$, $\delta = \sqrt{\frac{\gamma}{\alpha}}$, $M = 2$, $D_a = .15$, $N = 100$, $P_r = 3$, $E_c = 4$, $Q_0 = 1$, $S_c = .5$, $S_r = .3$ and $D_f = .1$ for various values of Q_0.

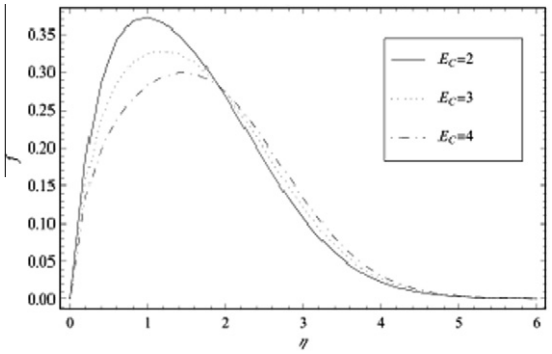

Figure 11 The velocity distribution is plotted vs. η, for a system having the parameters $\epsilon = .1$, $\tau = \frac{\pi}{5}$, $c = 1$, $\alpha = .8$, $\gamma = .4$, $\delta = \sqrt{\frac{\gamma}{\alpha}}$, $M = 2$, $D_a = .15$, $N = 100$, $P_r = 3$, $E_c = 4$, $Q_0 = 1$, $S_c = .5$, $S_r = .3$ and $D_f = .1$ for various values of E_c.

$$\frac{(\sqrt[3]{2}\xi_2 - b_1)}{3PrSc[3PrSc(\xi_1+\xi_2)]^{\frac{1}{3}}} + \frac{1}{3\sqrt[3]{2}PrS_c}(\xi_1+\xi_3)^{\frac{1}{3}} \leqslant 1 \tag{31}$$

where b_1, ξ_1, ξ_2 and ξ_3 are defined in the appendix.

The scheme is stable when the inequality (31) is satisfied. The local truncation error by employing the procedure used in Smith [12] is $O(\Delta\tau) + O(\Delta\eta)$ and it tends to zero as $\Delta\tau \to 0$ and $\Delta\eta \to 0$. Hence the scheme is compatible and then convergent, because compatibility and stability are necessary and sufficient conditions for convergence.

5. The skin-friction, heat and mass transfer

The skin-friction, heat and mass transfer in the non-dimensional form can be defined as

$$\tau_\omega = \left[\frac{\partial^2 f}{\partial\eta^2}\left(1 + \frac{\alpha}{\sqrt{\gamma\left(\frac{\partial f}{\partial\eta}\right)^2 + 1}}\right)\right]_{\eta=0} \tag{32}$$

$$Q = -\left[\frac{\partial\theta}{\partial\eta}\right]_{\eta=0} \tag{33}$$

$$S_t = -\left[\frac{\partial\psi}{\partial\eta}\right]_{\eta=0} \tag{34}$$

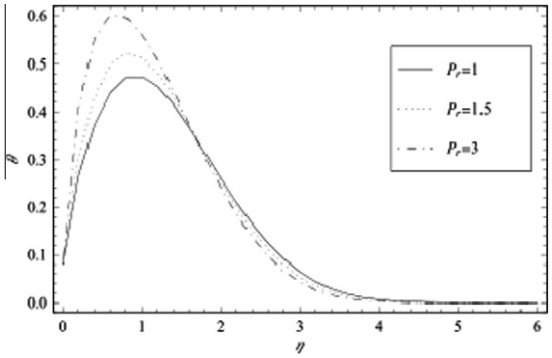

Figure 12 The temperature distribution is plotted vs. η, for a system having the parameters $\epsilon = .1$, $\tau = \frac{\pi}{5}$, $c = 1$, $\alpha = .8$, $\gamma = .4$, $\delta = \sqrt{\frac{\gamma}{\alpha}}$, $M = 2$, $D_a = .15$, $N = 100$, $P_r = 3$, $E_c = 4$, $Q_0 = 1$, $S_c = .5$, $S_r = .3$ and $D_f = .1$ for various values of P_r.

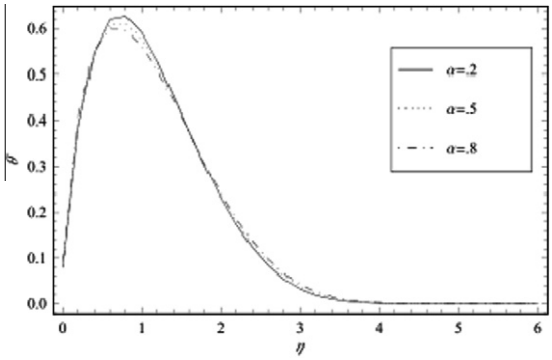

Figure 13 The temperature distribution is plotted vs. η, for a system having the parameters $\epsilon = .1$, $\tau = \frac{\pi}{5}$, $c = 1$, $\alpha = .8$, $\gamma = .4$, $\delta = \sqrt{\frac{\gamma}{\alpha}}$, $M = 2$, $D_a = .15$, $N = 100$, $P_r = 3$, $E_c = 4$, $Q_0 = 1$, $S_c = .5$, $S_r = .3$ and $D_f = .1$ for various values of α.

We can write Eqs. (32)–(34) by using finite difference method as follows:

$$\tau_\omega = \left(\frac{f_2^n - 2f_1^n + f_0^n}{(\Delta\eta)^2}\right)\left(1 + \frac{\alpha}{\sqrt{\gamma\left(\frac{f_1^n - f_0^n}{\Delta\eta}\right)^2 + 1}}\right) \tag{35}$$

$$Q = -\left(\frac{\theta_1^n - \theta_0^n}{\Delta\eta}\right) \tag{36}$$

$$S_t = -\left(\frac{\psi_1^n - \psi_0^n}{\Delta\eta}\right) \tag{37}$$

6. Results and discussion

Discussions of the numerical results are carried out to show the effects of the physical parameters entering the problem on the velocity of the fluid f, temperature θ, concentration ψ, the heat and mass transfer Q and S_t respectively. These effects were evaluated by setting $\omega = 1$, $\omega t = \frac{\pi}{5}$, $\gamma = 0.4$ and $\epsilon = 0.1$.

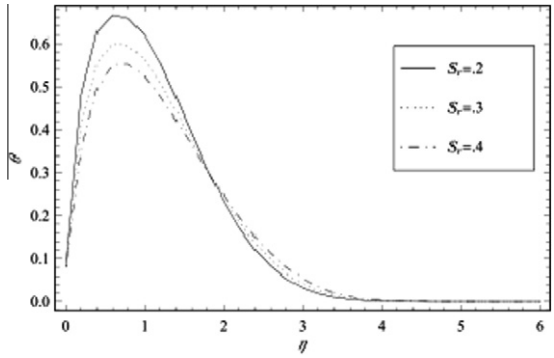

Figure 14 The temperature distribution is plotted vs. η, for a system having the parameters $\epsilon = .1$, $\tau = \frac{\pi}{5}$, $c = 1$, $\alpha = .8$, $\gamma = .4$, $\delta = \sqrt{\frac{\gamma}{\alpha}}$, $M = 2$, $D_a = .15$, $N = 100$, $P_r = 3$, $E_c = 4$, $Q_0 = 1$, $S_c = .5$, $S_r = .3$ and $D_f = .1$ for various values of S_r.

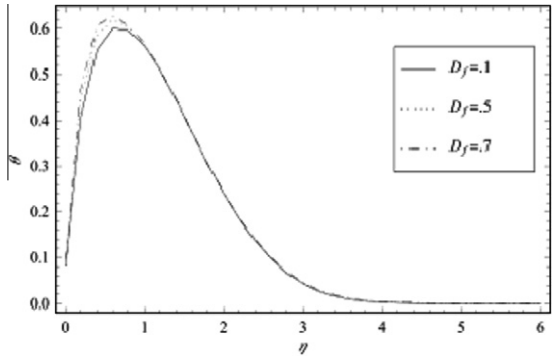

Figure 15 The temperature distribution is plotted vs. η, for a system having the parameters $\epsilon = .1$, $\tau = \frac{\pi}{5}$, $c = 1$, $\alpha = .8$, $\gamma = .4$, $\delta = \sqrt{\frac{\gamma}{\alpha}}$, $M = 2$, $D_a = .15$, $N = 100$, $P_r = 3$, $E_c = 4$, $Q_0 = 1$, $S_c = .5$, $S_r = .3$ and $D_f = .1$ for various values of D_f.

Figures 2–11 are plotted to illustrate the effect of different parameters on the velocity distribution f. It is observed that the velocity distribution decreases with the increase of the magnetic parameter M, which is obvious on Figure 2.

Figure 3 shows that the velocity distribution decreases as the non-Newtonian parameter α increases but at $\eta = 1$, it starts increasing with the increasing of α and at $\eta > 3$, it again increases as α increases. From Figs. 4 and 5, it is found that the velocity distribution f increases (or decreases) with the increasing of both Darcy number D_a and Prandtl number P_r. In Figure 6, it is found that f decreases with the increase of S_c. While from Figure 7, it is observed that an increase in D_f leads to decrease in the velocity distribution f. The effects of the Soret number S_r and buoyancy ratio parameter N are shown on Figs. 8 and 9. It is radically seen that the velocity increases (or decreases) with the increasing of both Sr and N. From Figs. 10 and 11, we see that the heat source parameter Q_0 and Eckert number E_c play a dual role. It is observed that the velocity distribution decreases with increasing the values of both Q_0 and E_c, but when $\eta = 1.8$, it increases as Q_0 and E_c increase.

Figs. 12–19 illustrate the effects of Prandtl number P_r, the non-Newtonian parameter α, Schmidt number S_c, Dufour number D_f, Soret number S_r, Eckert number E_c and the heat source parameter Q_0, in order, on the temperature distribution. Figure 12 shows that the temperature distribution increases with the increasing of P_r this occur near the plate, but an opposite effect occurs for $\eta > 1.8$. Figs. 13 and 14 show that the temperature distribution decreases as the non-Newtonian parameter α and Soret number S_r increase but at $\eta = 1.8$, it starts increasing with the increasing of α and S_r. From Figs. 15 and 16, It is observed that the temperature distribution increases with the increasing of both D_f and M. Figure 17 shows that an increase of Schmidt number S_c causes decrement in the temperature profile. Figs. 18 and 19 reveal the influence of Eckert number E_c and the heat source parameter Q_0 on the temperature distribution. It is observed that there is a rise in the temperature due to the heat created by the viscous dissipation and heat source. This result qualitatively agrees with expectations; since the effect of source and dissipation temperature is to increase the rate of energy transport to the fluid and accordingly increases the temperature of the fluid.

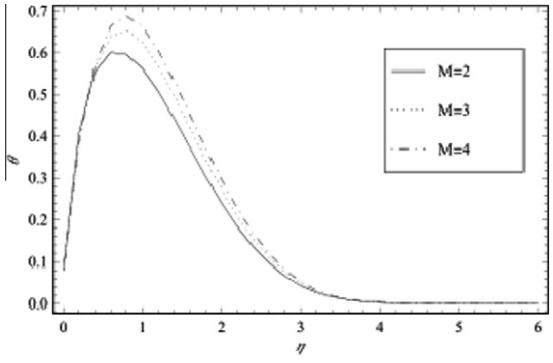

Figure 16 The temperature distribution is plotted vs. η, for a system having the parameters $\epsilon = .1$, $\tau = \frac{\pi}{5}$, $c = 1$, $\alpha = .8$, $\gamma = .4$, $\delta = \sqrt{\frac{\gamma}{\alpha}}$, $M = 2$, $D_a = .15$, $N = 100$, $P_r = 3$, $E_c = 4$, $Q_0 = 1$, $S_c = .5$, $S_r = .3$ and $D_f = .1$ for various values of M.

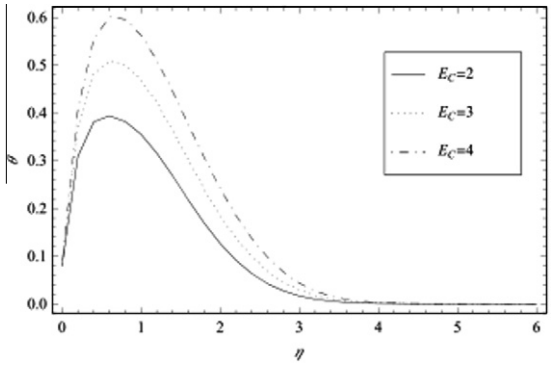

Figure 18 The temperature distribution is plotted vs. η, for a system having the parameters $\epsilon = .1$, $\tau = \frac{\pi}{5}$, $c = 1$, $\alpha = .8$, $\gamma = .4$, $\delta = \sqrt{\frac{\gamma}{\alpha}}$, $M = 2$, $D_a = .15$, $N = 100$, $P_r = 3$, $E_c = 4$, $Q_0 = 1$, $S_c = .5$, $S_r = .3$ and $D_f = .1$ for various values of E_c.

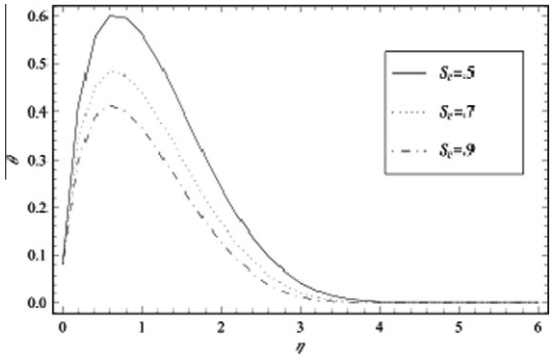

Figure 17 The temperature distribution is plotted vs. η, for a system having the parameters $\epsilon = .1$, $\tau = \frac{\pi}{5}$, $c = 1$, $\alpha = .8$, $\gamma = .4$, $\delta = \sqrt{\frac{\gamma}{\alpha}}$, $M = 2$, $D_a = .15$, $N = 100$, $P_r = 3$, $E_c = 4$, $Q_0 = 1$, $S_c = .5$, $S_r = .3$ and $D_f = .1$ for various values of S_c.

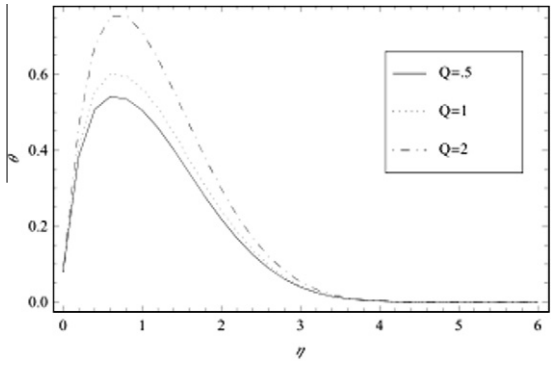

Figure 19 The temperature distribution is plotted vs. η, for a system having the parameters $\epsilon = .1$, $\tau = \frac{\pi}{5}$, $c = 1$, $\alpha = .8$, $\gamma = .4$, $\delta = \sqrt{\frac{\gamma}{\alpha}}$, $M = 2$, $D_a = .15$, $N = 100$, $P_r = 3$, $E_c = 4$, $Q_0 = 1$, $S_c = .5$, $S_r = .3$ and $D_f = .1$ for various values of Q_0.

The effects of α, D_a, E_c, S_r, D_f and S_c, on the concentration distribution are indicated in Figs. 20–25, respectively. Since the concentration distribution is a periodic function, then it will increase or decrease with the increase of the different parameters. From Figs. 20 and 21, it is found that the concentration distribution increases as α and P_r increase (or decrease) as shown in different regions. The effects of both the heat created by the viscous dissipation (Eckert number E_c) and Soret number S_r is to decrease the concentration profile, but when $\eta = 1.8$, it starts increasing as E_c and S_r increase as shown in Figs. 22 and 23. Figs. 24 and 25 show the effects of both Dufour number D_f and Schmidt number S_c on the concentration profiles. It is observed that the concentration decreases with increasing values of both D_f and S_c.

The values of heat transfer Q and mass transfer S_t are plotted vs. τ through Figs. 26–33 for various values of P_r, S_c, D_f and S_r. Figs. 26 and 27 show that the heat transfer increases and mass transfer decreases with increasing values of P_r for $\tau < 0.1\pi$, while the heat transfer decreases and mass transfer increases for $\tau > 0.1\pi$. From Figs. 28 and 29, it is observed that the heat transfer decreases and mass transfer increases with increasing values of D_f. In Figs. 30 and 31, we see that both of heat and mass transfer increase with the increasing of Schmidt number S_c. The effect of Soret number S_r on both of heat and mass transfer is to decrease them, but both of heat and mass transfer start increasing at $\tau = 0.2\pi$ and $\tau = 0.1\pi$ respectively, which is clearly depicted in Figs. 32 and 33.

Tables 1–3 presents numerical results for the functions $f''(0)$, $\theta'(0)$ and $-\psi'(0)$ which are representative of the skin friction, heat and mass transfer rate respectively, for various values of all parameters. It is clear from Table 1 that an increase in the non-Newtonian parameter $\hat{\alpha}$, Darcy number D_a and the magnetic parameter M give an increase in the values of dimensionless quantity $f''(0)$, but decreasing in the dimensionless quantity $-\theta'(0)$. Also, an increase in buoyancy ratio parameter N decreases the values of dimensionless quantities $f''(0)$ and $-\theta'(0)$ but increasing in the dimensionless quantity. In the case of the values of both $\hat{\alpha}$ and D_a increase, but M decreases, it is noted that the dimensionless quantity $-\psi'(0)$ increases.

From Table 2, in the case where the values of Prandtl number, Eckert number and heat source parameter increase, an increase in the values of dimensionless quantities $f''(0)$ and $-\psi'(0)$ but decreasing in the dimensionless quantity $-\theta'(0)$.

The values of $f''(0)$,$-\theta'(0)$ and $-\psi'(0)$ for various values of Schmidt number S_c, Soret number S_r and Dufour number D_f are presented in Table 3. It is noted that the dimensionless quantities $f''(0)$, $\theta'(0)$ and $\psi'(0)$ increase as S_c increases. Also, an increase in S_r and D_f gives an increase in the values of dimensionless quantities $f''(0)$ and $-\psi'(0)$ but decreasing in the dimensionless quantity $-\theta'(0)$.

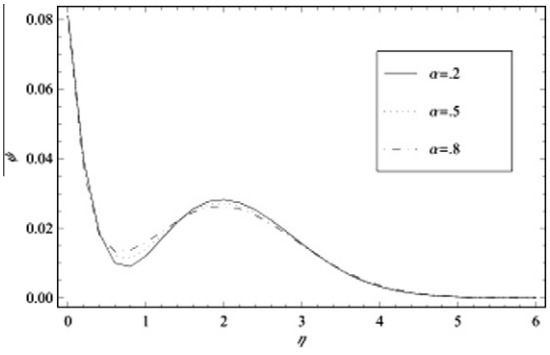

Figure 20 The concentration distribution is plotted vs. η, for a system having the parameters $\epsilon = .1$, $\tau = \frac{\pi}{5}$, $c = 1$, $\alpha = .8$, $\gamma = .4$, $\delta = \sqrt{\frac{\gamma}{\alpha}}$, $M = 2$, $D_a = .15$, $N = 100$, $P_r = 3$, $E_c = 4$, $Q_0 = 1$, $S_c = .5$, $S_r = .3$ and $D_f = .1$ for various values of α.

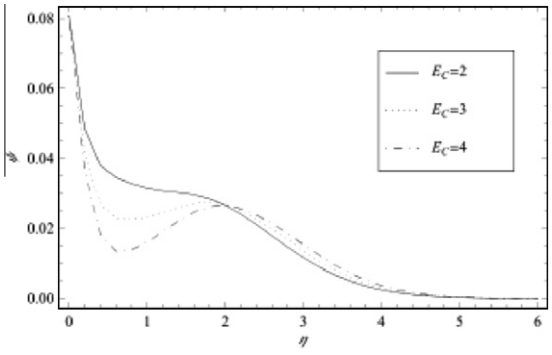

Figure 22 The concentration distribution is plotted vs. η, for a system having the parameters $\epsilon = .1$, $\tau = \frac{\pi}{5}$, $c = 1$, $\alpha = .8$, $\gamma = .4$, $\delta = \sqrt{\frac{\gamma}{\alpha}}$, $M = 2$, $D_a = .15$, $N = 100$, $P_r = 3$, $E_c = 4$, $Q_0 = 1$, $S_c = .5$, $S_r = .3$ and $D_f = .1$ for various values of E_c.

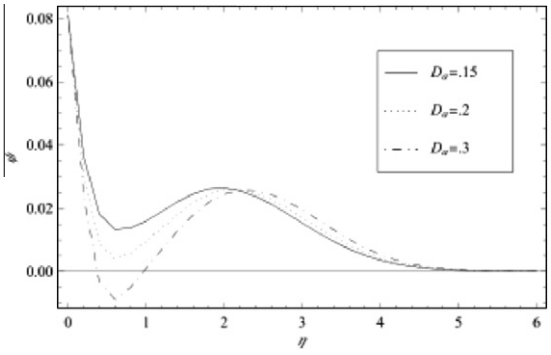

Figure 21 The concentration distribution is plotted vs. η, for a system having the parameters $\epsilon = .1$, $\tau = \frac{\pi}{5}$, $c = 1$, $\alpha = .8$, $\gamma = .4$, $\delta = \sqrt{\frac{\gamma}{\alpha}}$, $M = 2$, $D_a = .15$, $N = 100$, $P_r = 3$, $E_c = 4$, $Q_0 = 1$, $S_c = .5$, $S_r = .3$ and $D_f = .1$ for various values of P_r.

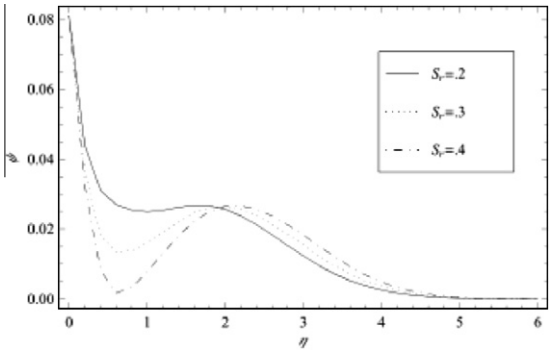

Figure 23 The concentration distribution is plotted vs. η, for a system having the parameters $\epsilon = .1$, $\tau = \frac{\pi}{5}$, $c = 1$, $\alpha = .8$, $\gamma = .4$, $\delta = \sqrt{\frac{\gamma}{\alpha}}$, $M = 2$, $D_a = .15$, $N = 100$, $P_r = 3$, $E_c = 4$, $Q_0 = 1$, $S_c = .5$, $S_r = .3$ and $D_f = .1$ for various values of S_r.

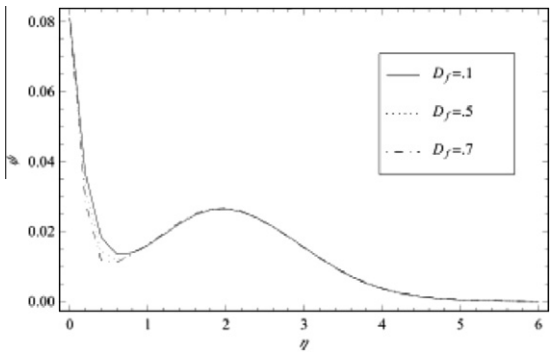

Figure 24 The concentration distribution is plotted vs. η, for a system having the parameters $\epsilon = .1$, $\tau = \frac{\pi}{5}$, $c = 1$, $\alpha = .8$, $\gamma = .4$, $\delta = \sqrt{\frac{\gamma}{\alpha}}$, $M = 2$, $D_a = .15$, $N = 100$, $P_r = 3$, $E_c = 4$, $Q_0 = 1$, $S_c = .5$, $S_r = .3$ and $D_f = .1$ for various values of D_f.

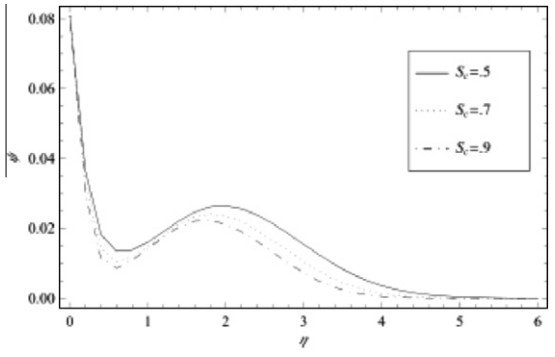

Figure 25 The concentration distribution is plotted vs. η, for a system having the parameters $\epsilon = .1$, $\tau = \frac{\pi}{5}$, $c = 1$, $\alpha = .8$, $\gamma = .4$, $\delta = \sqrt{\frac{\gamma}{\alpha}}$, $M = 2$, $D_a = .15$, $N = 100$, $P_r = 3$, $E_c = 4$, $Q_0 = 1$, $S_c = .5$, $S_r = .3$ and $D_f = .1$ for various values of S_c.

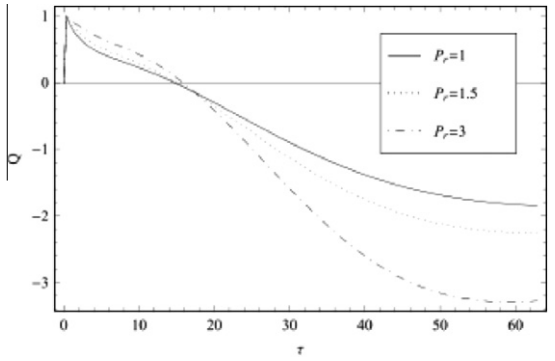

Figure 26 The heat transfer distribution is plotted vs. η, for a system having the parameters $\epsilon = .1$, $\tau = \frac{\pi}{5}$, $c = 1$, $\alpha = .8$, $\gamma = .4$, $\delta = \sqrt{\frac{\gamma}{\alpha}}$, $M = 2$, $D_a = .15$, $N = 100$, $P_r = 3$, $E_c = 4$, $Q_0 = 1$, $S_c = .5$, $S_r = .3$ and $D_f = .1$ for various values of P_r.

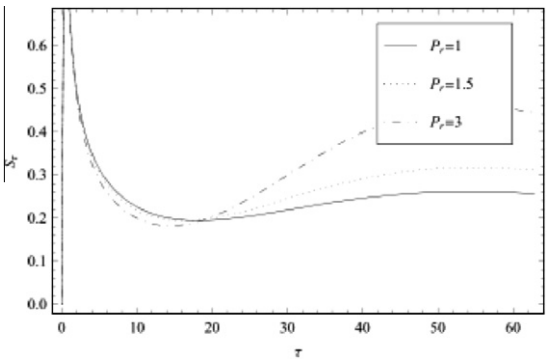

Figure 27 The mass distribution is plotted vs. η, for a system having the parameters $\epsilon = .1$, $\tau = \frac{\pi}{5}$, $c = 1$, $\alpha = .8$, $\gamma = .4$, $\delta = \sqrt{\frac{\gamma}{\alpha}}$, $M = 2$, $D_a = .15$, $N = 100$, $P_r = 3$, $E_c = 4$, $Q_0 = 1$, $S_c = .5$, $S_r = .3$ and $D_f = .1$ for various values of P_r.

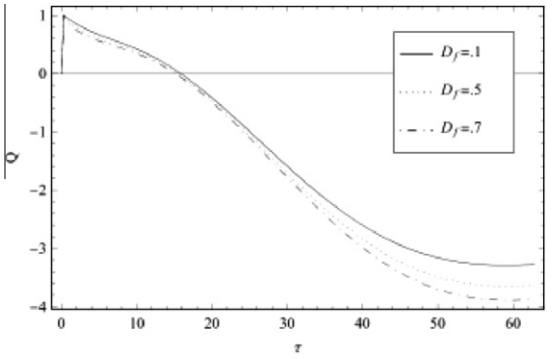

Figure 28 The heat transfer distribution is plotted vs. η, for a system having the parameters $\epsilon = .1$, $\tau = \frac{\pi}{5}$, $c = 1$, $\alpha = .8$, $\gamma = .4$, $\delta = \sqrt{\frac{\gamma}{\alpha}}$, $M = 2$, $D_a = .15$, $N = 100$, $P_r = 3$, $E_c = 4$, $Q_0 = 1$, $S_c = .5$, $S_r = .3$ and $D_f = .1$ for various values of D_f.

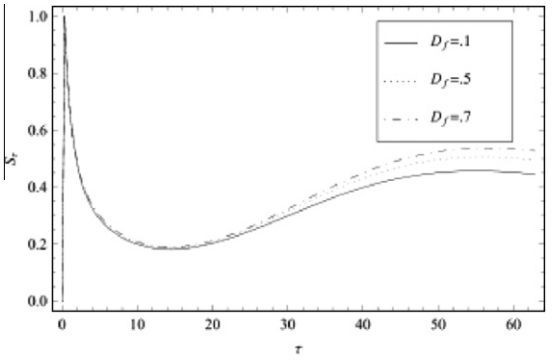

Figure 29 The mass transfer distribution is plotted vs. η, for a system having the parameters $\epsilon = .1$, $\tau = \frac{\pi}{5}$, $c = 1$, $\alpha = .8$, $\gamma = .4$, $\delta = \sqrt{\frac{\gamma}{\alpha}}$, $M = 2$, $D_a = .15$, $N = 100$, $P_r = 3$, $E_c = 4$, $Q_0 = 1$, $S_c = .5$, $S_r = .3$ and $D_f = .1$ for various values of D_f.

7. Conclusion

The explicit-finite difference method is used to compute the effects of the external forces on coupled heat and mass transfer equations for a non-Newtonian fluid flowing through a porous medium obeying Darcy's law and periodically heated from below. The non-Newtonian fluid used is Eyring–Powell model.

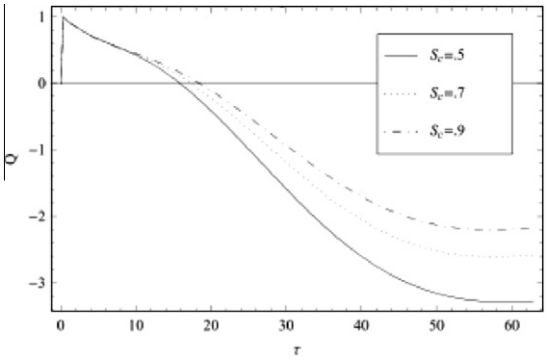

Figure 30 The heat transfer distribution is plotted vs. η, for a system having the parameters $\epsilon = .1$, $\tau = \frac{\pi}{5}$, $c = 1$, $\alpha = .8$, $\gamma = .4$, $\delta = \sqrt{\frac{\tau}{\alpha}}$, $M = 2$, $D_a = .15$, $N = 100$, $P_r = 3$, $E_c = 4$, $Q_0 = 1$, $S_c = .5$, $S_r = .3$ and $D_f = .1$ for various values of S_c.

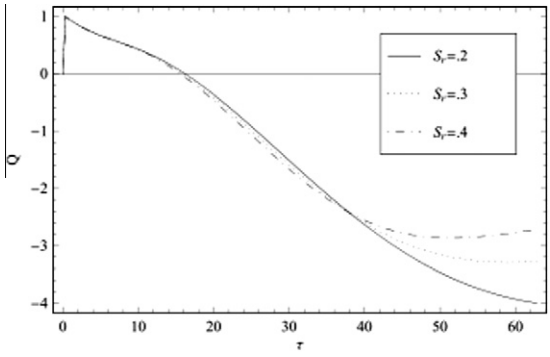

Figure 32 The heat transfer distribution is plotted vs. η, for a system having the parameters $\epsilon = .1$, $\tau = \frac{\pi}{5}$, $c = 1$, $\alpha = .8$, $\gamma = .4$, $\delta = \sqrt{\frac{\tau}{\alpha}}$, $M = 2$, $D_a = .15$, $N = 100$, $P_r = 3$, $E_c = 4$, $Q_0 = 1$, $S_c = .5$, $S_r = .3$ and $D_f = .1$ for various values of S_r.

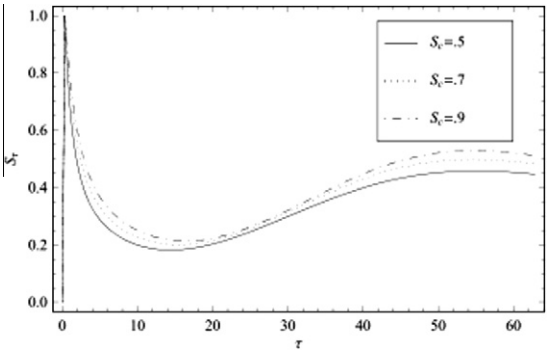

Figure 31 The mass transfer distribution is plotted vs. η, for a system having the parameters $\epsilon = .1$, $\tau = \frac{\pi}{5}$, $c = 1$, $\alpha = .8$, $\gamma = .4$, $\delta = \sqrt{\frac{\tau}{\alpha}}$, $M = 2$, $D_a = .15$, $N = 100$, $P_r = 3$, $E_c = 4$, $Q_0 = 1$, $S_c = .5$, $S_r = .3$ and $D_f = .1$ for various values of S_c.

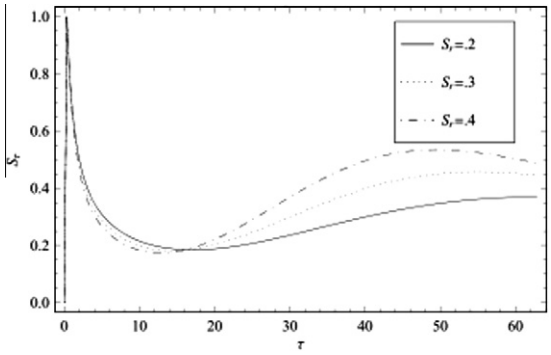

Figure 33 The mass transfer distribution is plotted vs. η, for a system having the parameters $\epsilon = .1$, $\tau = \frac{\pi}{5}$, $c = 1$, $\alpha = .8$, $\gamma = .4$, $\delta = \sqrt{\frac{\tau}{\alpha}}$, $M = 2$, $D_a = .15$, $N = 100$, $P_r = 3$, $E_c = 4$, $Q_0 = 1$, $S_c = .5$, $S_r = .3$ and $D_f = .1$ for various values of S_r.

The system is influenced by an external uniform magnetic field and a heat source. This work is an extension of Kafoussias [7].

In this study, the governing non-linear partial differential equations are transformed into system of algebraic non-linear

Table 1 Numerical results for the skin friction, for various values of all parameters

$\hat{\alpha}$	M	D_a	N	$f''(0)$	$-\Theta'(0)$	$-\Psi'(0)$
0.2	2	0.15	100	−17.1397	−1.68165	0.30156
0.5	2	0.15	100	−16.5195	−1.71449	0.30806
0.8	2	0.15	100	−16.2637	−1.75303	0.315159
0.1	2	0.15	100	−16.2637	−1.75303	0.315159
0.1	3	0.15	100	−16.2037	−1.79708	0.314549
0.1	4	0.15	100	−16.1085	−1.83492	0.309281
0.1	2	0.15	100	−16.2637	−1.75303	0.315159
0.1	2	0.2	100	−16.0204	−2.12066	0.354251
0.1	2	0.3	100	−12.9001	−2.59304	0.404212
0.1	2	0.15	100	−16.2637	−1.75303	0.315159
0.1	2	0.15	115	−16.9934	−2.28751	0.374182
0.1	2	0.15	130	−17.3158	−2.84083	0.436229

Table 2 Numerical results for the heat mass transfer, for various values of all parameters

E_c	P_r	Q_0	$f''(0)$	$-\Theta'(0)$	$-\Psi'(0)$
2	3	1	−18.0394	−0.810661	0.246037
3	3	1	−17.1402	−1.29469	0.265207
4	3	1	−16.2637	−1.75303	0.315159
4	1	1	−18.1719	−0.975178	0.222993
4	1.5	1	−17.5867	−1.22894	0.252406
4	3	1	−16.2637	−1.75303	0.315159
4	3	0.5	−16.4195	−1.65824	0.305645
4	3	1	−16.2637	−1.75303	0.315159
4	3	2	−15.9246	−1.96311	0.335998

Table 3 Numerical results for the mass transfer, for various values of all parameters

S_c	S_r	D_f	$f''(0)$	$-\Theta'(0)$	$-\Psi'(0)$
0.5	0.3	0.1	−16.2637	−1.75303	0.315159
0.7	0.3	0.1	−16.175	−1.32868	0.332237
0.9	0.3	0.1	−16.1306	−1.05632	0.339799
0.5	0.2	0.1	−17.6758	−1.68156	0.245472
0.5	0.3	0.1	−16.2637	−1.75303	0.315159
0.5	0.4	0.1	−14.67	−1.82259	0.391538
0.5	0.3	0.1	−16.2637	−1.75303	0.315159
0.5	0.3	0.5	−15.9103	−1.88824	0.332646
0.5	0.3	0.7	−15.7014	−1.96675	0.342822

equations by using finite difference method. The numerical results indicate that as the non-Newtonian and magnetic parameters increase, the value of the velocity decreases. This conclusion meets the logic of the magnetic field exerting a retarding force on the free convection flow. Moreover, it is noted that there is a rise in the temperature due to the heat created by the viscous dissipation, free convection and heat source, but the concentration increases (or decreases) as Eckert number, buoyancy ratio and volumetric rate of heat generation increase. Also, the effect of the non-Newtonian parameter is to decrease (or increase) the temperature and the concentration. This problem has many scientific and engineering applications such as

(a) Flow of blood through the arteries.
(b) Soil mechanics, water purification, and powder metallurgy.
(c) Study of the interaction of the geomagnetic field with in the geothermal region.
(d) The petroleum engineer concerned with the movement of oil, gas and water through the reservoir of an oil or gas field.

It is hoped that the present work will serve as a vehicle for understanding more complex problems involving the various physical effects investigated in the present problem.

Appendix A.

$$A_1 = 1 + \gamma\alpha_3 - \alpha_1$$

$$A_2 = 1$$

$$A_3 = N$$

$$A_4 = \gamma_2\left[\alpha_2 + \tfrac{1}{\delta} sinh^{-1}\left(\sqrt{\gamma}\alpha_2\right)\right] - (\Delta\tau) M E_c |f_i^n|$$

$$A_5 = 1 + \tfrac{2}{P_r}\gamma_1 + Q$$

$$A_6 = 2D_f\gamma_1$$

$$A_7 = 2S_r\gamma_1$$

$$A_8 = 1 + \tfrac{2}{S_c}\gamma_1$$

$$\alpha_1 = (\Delta\tau)\left(M + \tfrac{1}{D_a}\right)$$

$$\alpha_2 = \left|\tfrac{f_{i+1}^n - f_1^n}{\Delta\eta}\right|$$

$$\alpha_3 = 1 + \tfrac{\hat{\alpha}}{\sqrt{\gamma\alpha_2^2 + 1}}$$

$$\gamma_1 = \tfrac{2(\Delta\tau)}{(\Delta\eta)^2}(cos\phi - 1)$$

$$\gamma_2 = E_c\left(\tfrac{\Delta\tau}{\Delta\eta}\right)(e^{I\phi} - 1)$$

$$b_1 = PrSc\delta(3 + Q_0 - \alpha_1 + \alpha_3\gamma_3) + 2\gamma_1\delta(Pr + Sc)$$

$$b_2 = PrSc\delta(3 + 2Q_0 - 2\alpha_1 + Ec|f_i^n|M\Delta\tau - \alpha_1 Q_0 + 2\alpha_3\gamma_1 + \alpha_3\gamma_1 Q_0 - \alpha_2\gamma_2) - PrSc\gamma_2 sinh^{-1}(\sqrt{\gamma\alpha_2}) + 2\gamma_1\delta Pr(2 + Q_0 - \alpha_1 - 2D_f SrSc\gamma_1 + \alpha_1\gamma_1) + Sc(2 - \alpha_1 + \alpha_3 + 2\gamma_1)$$

$$b_3 = Pr^3 Q_0^2 Sc^3\delta^3(2Q_0 + 3\alpha_1) + 9EcPr^3 Sc^3\delta^3|f_i^n|M\Delta\tau(Q_0 - \alpha_1)$$
$$b_4 = Pr^3 Sc^3\delta^3(3Q_0 - 2\alpha_1) - 6Pr^2 Q_0^2 Sc^2\delta^3\gamma_1(Pr - 2Sc)$$
$$b_5 = -18EcPr^2 Sc^2\delta^3|f_i^n|M\gamma_1\Delta\tau(2Pr - Sc - 3NPrScSr)$$
$$b_6 = 6Pr^3 Sc^2\delta^3\alpha_1\gamma_1(4Q_0 - \alpha_1) + 6Pr^2 Sc^3\Delta^3\alpha_1\gamma_1(2Q_0 - \alpha_1)$$

$$b_7 = 3Pr^3 Sc^3\delta^3\alpha_3\gamma_1\left(Q_0^2 + 3Ec|f_i^n|M\Delta\tau + 2Q_0\alpha_1\right)$$
$$b_8 = 6Pr^2 Sc^2\delta^3\gamma_1\left(PrSc\alpha_3\alpha_1^2 - 4Q_0\gamma_1\right) - 12PrScQ_0\delta^3\gamma_1^2(Pr^2 - 2Sc^2)$$
$$b_9 = 12Pr^2 Sc^2\delta^3\gamma_1^2(3D_f PrScSrQ_0 - 4\alpha_1) + 12PrSc\alpha_1\delta^3\gamma_1^2(Pr^2 + Sc^2)$$
$$b_{10} = 12Pr^2 Sc^2\delta^3\gamma_1^2(3D_f PrScSr\alpha_1 + 2PrQ_0\alpha_3 - ScQ\alpha_3)$$
$$b_{11} = -3Pr^2 Sc^2\delta^3\gamma_1^2\alpha_3(4Pr\alpha_1 - 4ScQ_0\alpha_3 + 2PrSc\alpha_3\alpha_1)$$
$$b_{12} = 4\delta^3\gamma_1^3(4Pr^3 - 6Pr^2 Sc - 6PrSc^2 + 4Sc^3)$$

$$b_{13} = 72Pr^2 Sc^2\delta^3 D_f Sr(Pr + Sc) - 12Pr^2 Sc\alpha_3\delta^3\gamma_1^3(Pr - Sc),$$
$$b_{14} = -12PrSc^3\delta^3\gamma_1^3\alpha_3(1 + 6Pr^2 D_f Sr) - Pr^2 Sc^2\alpha_3^2\delta^3\gamma_1^3(Pr + Sc)$$
$$b_{15} = 2Pr^3 Sc^2\delta^3\gamma_1(Sc\alpha_3^3\gamma_1^2 - 18\alpha_2\gamma_2) + 9Pr^3 Sc^3\alpha_2\gamma_2\delta^3(Q_0 - \alpha_1)$$
$$b_{16} = 9Pr^2 Sc^3\alpha_2\gamma_1\gamma_2\delta^3(2 + 6NPrSr + Pr\alpha_3)$$

$$b_{17} = 9Pr^2 Sc^2\gamma_2\delta^2 sinh^{-1}(\sqrt{\gamma\alpha_2})(PrScQ_0 - PrSc\alpha_1 - 4Pr\gamma_1 + 2Sc\gamma_1 + 6NPrScSr\gamma_1 + PrSc\alpha_3\gamma_1)$$

$$\xi_1 = \sum_{i=3}^{17} b_i, \qquad \xi_2 = b_1^2 + 3PrSc\delta b_2, \qquad \xi_3 = \xi_1^2 + 4\xi_2^3$$

References

[1] M.A. Abd El-Naby, E.M.E. Elbarbary, N.Y. Abdelazem, Finite difference solution of radiation effects on MHD unsteady free-convection flow over vertical plate with variable surface temperature, J. Appl. Math. 2 (2003) 65.

[2] E.R.G. Eckert, R.M. Drake, Analysis of Heat and Mass Transfer, McGrawHill Kogakusha, Ltd, 1972.

[3] N.T. Eldabe, A.G. El-Sakka, A. Fouad, Numerical treatment of MHD convective heat and mass transfer in an electrically conducting fluid over an infinite solid surface in presence of the internal heat generation, Z. Naturfosch 58 (2003) 601.

[4] N.T. Eldabe, Magnetohydrodynamic unsteady free-convective flow through a porous medium bounded by an infinite vertical porous plate, Can. J. Phys. 64 (1986) 949.

[5] N.T. Eldab, M.A. Abd El-Naby, Fouad. Ashraf, Sayed. Amaney, Numerical study of the flow of magnetohydrodynamic non-Newtonian fluid obeying the Eyring–Powell model through a non-Darcy porous medium with coupled heat and mass transfer, J. Porous Media 11 (7) (2008) 691.

[6] D. Ingham, I. Pop, (Eds.), Transport phenomena in porous media, Pergamon, Oxford, vol. I (1998), vol. II (2002).

[7] N.G. Kafoussias, The effects of mass transfer on free convective flow of a viscous and incompressible fluid past a vertical isothermal cone surface, Int. J. Eng. Sci. 30 (1992) 273.

[8] Y.J. Kim, A.G. Fedorov, Transient mixed radiative convection flow of a micropolar fluid past a moving semi-infinite vertical porous plate, Int. J. Heat Mass Transfer 46 (2003) 1751.

[9] D.A. Nield, A. Bejan, Convection in Porous Media, second ed., Springer, New York, 1999.

[10] I. Pop, D. Ingham, Convective heat transfer: mathematical and computational modelling of viscous fluids and porous media, Pergamon, Oxford, 2001.

[11] M.A. Seddeek, Thermal radiation and buoyancy effects on MHD free convective heat generating flow over an accelerating permeable surface with temperature-dependent viscosity, Can. J. Phys. 79 (2001) 725.

[12] G.D. Smith, Numerical Solution of Partial Differential Equations, Oxford University press, New York, 1985.

[13] V.M. Soundalgekar, P. Ganesan, An implicit finite difference analysis of transient free convective flow past a semi-infinite vertical flat plate, Int. J. Eng. Sci. 19 (1981) 757.

[14] O.V. Trevisan, A. Bejan, Natural convection phenomena occurring inside a porous layer with both heat and mass transfer from the side, Int. J. Heat Mass Transfer 28 (1985) 1597.

[15] K. Vafai (Ed.), Handbook of Porous Media, Marcel Dekker, New York, 2000.

[16] K. Vajravelu, A. Hadjinicolaou, Convective heat transfer in an electrically conducting fluid at a stretching surface with uniform free stream, Int. J. Eng. Sci. 35 (12) (1997) 1237.